Journal of Power Sources 227 (2013) 145–152

Contents lists available at SciVerse ScienceDirect

Journal of Power Sources

journal homepage: www.elsevier.com/locate/jpowsour

Effect of samarium content on onset of minor p-type conductivity in ceria-based electrolytes

D. Pérez-Coll [a,*], P. Núñez [b], J.R. Frade [c]

[a] Instituto de Cerámica y Vidrio (CSIC), Cantoblanco, 28049 Madrid, Spain
[b] Dep. Química Inorgánica, Universidad de La Laguna, 38200 La Laguna, Tenerife, Spain
[c] Dep. Engenharia de Materiais e Cerâmica, CICECO Universidade de Aveiro, 3810-193 Aveiro, Portugal

HIGHLIGHTS

- Effect of Sm content on the electrochemical permeability of ceria-based electrolytes.
- Prevailing ionic conducting character under oxidising conditions.
- Oxygen flux by permeation related to the onset of minor electronic conductivity.
- P-type conductivity extend active surface for electrochemical interchange in air electrodes.

ARTICLE INFO

Article history:
Received 13 September 2012
Received in revised form
12 November 2012
Accepted 20 November 2012
Available online 27 November 2012

Keywords:
Ceria-based electrolytes
Mixed conduction
Oxidizing conditions
Electrochemical permeability
p-type electronic conductivity

ABSTRACT

$Ce_{1-x}Sm_xO_{2-\delta}$ powders ($x = 0.1, 0.2, 0.3$) were prepared by a freeze-drying method, preserving monophasic fluorites when precursors were annealed between 375 and 1600 °C. Dried precursor powders were calcined at 375 °C for 4 h and sintered at 1600 °C for 10 h yielding gas-tight ceramics with densifications >95%. The oxygen-electrochemical permeability measurements were employed to study the oxygen flux under moderate oxidizing conditions which was directly related to the onset of residual electronic conductivity. In the experimental process the charge transport through the membrane was due to the ambipolar conductivity, which was controlled by the minor electronic conductivity in $Ce_{1-x}Sm_xO_{2-\delta}$. The electronic properties of the pellets were analysed between $pO_2 \approx 10^{-3}$–0.21 atm in the range 750–900 °C. The estimated ionic transport number, obtained by combination of the electronic conductivity by oxygen permeability and total conductivity by impedance spectroscopy, remained higher than 0.99 in the studied conditions. The electronic conductivity was found dominated by p-type carriers and dependent on the content of Sm in the ceria lattice. Although the overall electrical conductivity under oxidizing conditions is governed by the ionic behaviour, an increased Sm-doping improved the p-type conductivity.

1. Introduction

High-temperature electrochemical devices have received a growing interest in current days due to the favourable kinetics of the electrochemical reactions prosper the high efficiency of the whole processes [1–5]. Many of these applications as solid oxide fuel cells, solid oxide electrolyzers, oxygen pumps or oxygen sensors require the use of a ceramic electrolyte with suitable oxide-ion conductivity. The state of the art electrolyte in high temperature (800–1000 °C) devices is yttrium-stabilized zirconia (YSZ) due to its relatively high ionic conductivity, negligible electronic conductivity, good stability and good mechanical properties [1,6,7]. However current trend is to decrease the operating temperature to intermediate range (500–700 °C) to overcome problems related to the stability and degradation of the components [8–10]. Given that YSZ possesses poorer electrical properties in this interval of working temperature, alternative solid electrolytes as ceria-based oxides have been widely studied because of their superior ionic conductivity compared with the former [2,11,12]. The ionic conductivity is established by the creation of mobile oxygen vacancies in the lattice of CeO_2-based materials by additions of trivalent cations in the Ce^{4+} position [13,14]. The most extensively used additives are rare earth cations as Gd^{3+}, Sm^{3+}, La^{3+} and Y^{3+} which present a high solubility in the ceria lattice due to good

* Corresponding author. Tel.: +34 917 355 840; fax: +34 917 355 843.
E-mail addresses: dpcoll@icv.csic.es, dpcoll@ull.es (D. Pérez-Coll).

0378-7753/$ – see front matter © 2012 Elsevier B.V. All rights reserved.
http://dx.doi.org/10.1016/j.jpowsour.2012.11.064

matching of ionic radii between the host and the dopant [13]. Although the main problem of ceria based compounds comes from the high reducibility of Ce^{4+} to Ce^{3+} at low pO_2, which results in considerable n-type electronic conductivity, this is alleviated at intermediate temperature due to the relatively high enthalpy of reduction [8]. However, reducing operating temperature from high to intermediate range worsens the kinetics of the electrochemical reactions which increases the electrode polarization resistance and harms the performance of SOFC and other electrochemical systems. As an interesting feature, it has been reported that the electronic conductivity around the interface of reaction has a positive impact in the improvement of the electrode performance [15–17]. Regarding this, it has been stated that the charge-transfer reaction is the rate-limiting step in the oxygen-reduction reaction [18,19], which points to the presence of electronic species capable of reaching active sites at the interface as a crucial key to improve the cathode performance. The defect chemistry model of ceria-based compounds predicts wide changes in the charge-transport properties with variations in the content of the dopant. The ionic conductivity of the bulk increases with increasing fractions of the acceptor-type additives fraction until reaching a maximum, then decreasing for higher contents [8,20–23]. The reasons for this behaviour are ascribed to the increase of defect associates as $(Ln'_{Ce}\cdot V_O^{\bullet\bullet})^{\bullet}$ for high contents of aliovalent additive, which restricts the concentration of free-oxygen vacancies (note that Ln'_{Ce} corresponds to the lanthanide dopant in the Ce^{4+} position and $V_O^{\bullet\bullet}$ to the oxygen vacancy). Also it has been reported that samples with lower contents of trivalent dopant in the CeO_2 lattice are more affected by resistive grain boundaries, consistent with a stronger effect of space charge layer [22–24]. Less attention has been paid to the effect of dopant content on the electronic properties, which are strongly influenced by the oxygen partial pressure given that the equilibrium with the environment affects the content of the charge carriers. The main reasons probably stem from actual issues in the separation between the ionic and the electronic contributions, which requires specific and elaborated techniques [25–28].

In previous works we reported significant effects of the Gd and Sm fractions on the n-type electronic conductivity under reducing conditions [29,30] which was directly related to differences in the reducibility with the dopant content [29]. In the present work we study the mixed conducting behaviour of $Ce_{1-x}Sm_xO_{2-\delta}$ ($x = 0.1$, 0.2, 0.3) under oxidizing conditions. The oxygen-electrochemical-permeability technique is used to obtain the oxygen flux and minor p-type electronic conductivity, whereas the overall conductivity is obtained from impedance spectroscopy data. Experimental results from both techniques are combined to obtain the ionic transport number for different compositions.

2. Experimental

Nanometric powders corresponding to the solid solution $Ce_{1-x}Sm_xO_{2-\delta}$ ($x = 0.1, 0.2, 0.3$) were prepared by freeze drying [30]. Aqueous solutions with stoichiometric amounts of cerium and samarium, coming from nitrates $Ce(NO_3)_3\cdot 6H_2O$ (Aldrich, 99.99%) and $Sm(NO_3)_3\cdot 6H_2O$ (Aldrich, 99.9%), were flash frozen in liquid nitrogen and dehydrated for 3 days in a freeze drier (Heto Lyolab 3000). These as prepared precursor powders were calcined at 375 °C for 4 h and ground in a ball milling with zirconia-based balls to break the aggregates. Crystalline phases were analysed by XRD with a Philip's X'pert powder diffractometer with Cu Kα radiation, equipped with a graphite secondary monochromator.

Compacted samples were prepared by uniaxially pressing the powders in a cylindrical punch and sintered at 1600 °C for 10 h. The apparent density of the samples was calculated from the mass to geometric volume ratio and compared with the theoretical density of each composition to obtain the % densification. The theoretical density correponds to the density of the single cell, obtained through the unit cell parameter extracted by Rietveld refinement of the XRD data of sintered samples.

The mixed conducting behaviour of sintered disks under moderate oxidizing conditions was studied by oxygen-electrochemical permeability following the procedure reported elsewhere [28,31–33]. The experimental method (Fig. 1) is based on submitting both sides of the sintered pellets to a moderate gradient of oxygen partial pressure and analyse the current flux through the samples caused by the mixed conduction properties. For this purpose, an electrochemical cell which comprises an oxygen pump and an oxygen-partial-pressure sensor is constructed. The mixed-conducting samples were sealed against the top of a YSZ tube which acts as the electrochemical pump by removing the oxygen from inside the cell, thus decreasing the oxygen partial pressure. The bottom of the tube is sealed over a YSZ sintered pellet which controls the oxygen-partial pressure inside the cell (pO_2) by the voltage difference between both sides of the pellet (V_0) according to the Nernst equation:

$$V_0 = \frac{RT}{4F}\cdot \ln\left(\frac{pO_2^*}{pO_2}\right) \quad (1)$$

where pO_2^* is the outer oxygen partial pressure which remains constant ~0.21 atm; R, T and F have their usual meanings. The inner and outer faces of the YSZ tube and YSZ pellet were covered with Pt electrodes and attached to Pt wires for electrical contacts and to allow the electrochemical reactions. The slightly reducing conditions inside the cell were obtained by increasing the cathodic polarization in the inner electrode of the pump by the application of voltages from a d.c source (Yokogawa 7651) in the range 20–200 mV with steps of 20 mV, in the temperature range 750–900 °C. A Keithley 2700 + 7700 d.c. multimeter was used to read the voltage drops in the sensor and in an external resistance in series with the pump, which was used to obtain the pumped current, and to extract the corresponding values of permeability. In order to improve the kinetics of the electrochemical reactions Pt electrodes were also applied to both the inner and the outer surfaces of the samples. For this purpose both faces were coated with Pt paste by painting and then the samples were annealed at 950 °C for 1 h to remove the organic content and improve porosity of the electrodes.

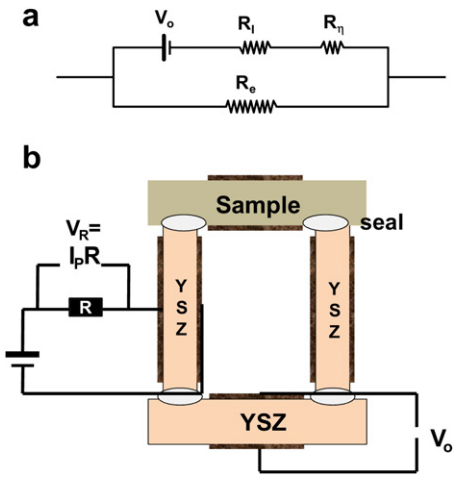

Fig. 1. (a) Equivalent circuit representing the mixed conducting membrane and (b) experimental cell for electrochemical permeability measurements.

3. Results

3.1. Structural and microstructural characterization

The freeze-drying procedure yields dried and amorphous precursors which have to be calcined to decompose organic residues. Complete decomposition is expected at temperatures lower than 400 °C, as confirmed by TG/DTA [34]. Dried precursors were, thus, calcined at 375 °C for 4 h and XRD measurements confirmed the presence of single phase fluorite (Fig. 2(a)). Phase purity was also retained by sintering at 1600 °C for 10 h (Fig. 2(b)) with a nearly linear increase in unit cell parameter versus samarium content, as previously reported [30]. Sintered bodies are gas tight, with densification >95%, to avoid the diffusion of O_2-gas phase through residual porosity of ceramic samples, and to ensure that permeation is strictly electrochemical.

3.2. Oxygen permeability and p-type electronic conductivity

On assuming perfect gas sealing and since the electrochemical permeability of YSZ cell components is very low the oxygen flux through the mixed conducting material is nearly identical to the oxygen flux through the YSZ-electrochemical pump [31]:

$$j_{O_2} \approx \frac{I_p}{4FA} \tag{2}$$

where L is the thickness and A is the area the of the mixed conducting membrane. Fig. 3 shows representative results of the

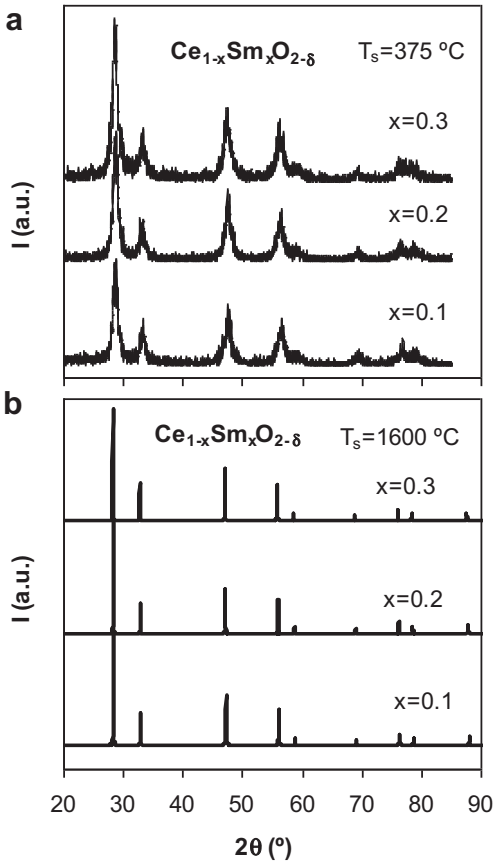

Fig. 2. X-ray diffraction data of $Ce_{1-x}Sm_xO_{2-\delta}$ (x = 0.1, 0.2, 0.3) (a) after calcining freeze-drying precursors at 375 °C for 4 h and (b) after annealing calcined powders at 1600 °C for 10 h.

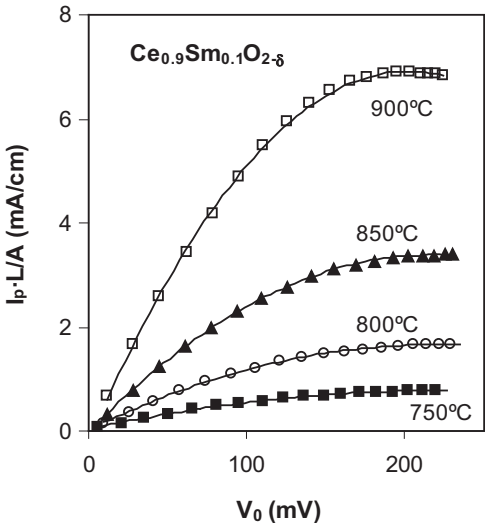

Fig. 3. Current of permeability as a function of the voltage drop between both sides of the pO_2 sensor for $Ce_{0.9}Sm_{0.1}O_{1.95-\delta}$. Lines represent the fitting of the experimental data to a polynomial solution.

pumped current (I_p), which corresponds to electrochemical permeability through the ceria-based membranes, as a function of the Nernst reading obtained by the pO_2 probe. The electrochemical permeability relies on the mixed oxygen-ionic-electronic conduction of ceria-based materials, assuming that gas-tight samples are submitted to a gradient of oxygen partial pressure [32,35], yielding the ambipolar conductivity:

$$\sigma_{amb} = \frac{\sigma_i \cdot \sigma_e}{\sigma_i + \sigma_e} \tag{3}$$

where σ_i and σ_e are the ionic and the electronic conductivities, respectively. Electrochemical permeation corresponds to combined transport of ionic and electronic species, coupled by charge transfer reactions at the surfaces. If surface exchange and gas phase transport limitations are negligible the current of permeability is directly related to the ambipolar conductivity according to [36,37]:

$$\sigma_{amb} = \frac{L}{A}\frac{dI_p}{dV_0} \tag{4}$$

Eq. (4) assumes that overpotentials at the electrodes are negligible compared to the theoretical electromotive force created by differences in oxygen partial pressure in both sides of the cell. However, electrochemical reactions at the electrodes could produce considerable values of electrode polarization resistance in current working conditions. Actually, this may yield underestimated values of ambipolar conductivity, as found analysing the equivalent circuit shown in Fig. 1, according to:

$$\sigma_{amb} \approx \frac{L}{A}\frac{dI_p}{dV_0} \Big/ \left(1 - R_\eta \frac{dI_p}{dV_0}\right) \approx \frac{L}{A}\frac{dI_p}{dV_0}(1+\delta) \tag{5}$$

where

$$\delta = \frac{R_\eta A}{L}\sigma_{amb} \tag{6}$$

At moderate oxidizing conditions one could estimate values of electrode polarization resistance by impedance spectroscopy in air in the range 1.50–0.25 Ω cm^2 for 750–900 °C for different compositions. These would yield values of ambipolar conductivity

using Eq. (5) only about 0.1–0.2% higher than those obtained with Eq. (4).

Combining Eq. (1)–(4) the oxygen flux density as a function of the ambipolar conductivity is expressed as:

$$j_{O_2} = \frac{RT}{16F^2L}\int_{\ln pO_2}^{\ln pO_2*} \sigma_{amb}\cdot d(\ln pO_2) \quad (7)$$

and, for a given oxygen-partial-pressure gradient, Eq. (7) is approximated as:

$$j_{O_2} = \frac{RT}{16F^2L}\sigma_{amb}^{av}\ln\left(\frac{pO_2^*}{pO_2}\right) \quad (8)$$

where σ_{amb}^{av} is the ambipolar conductivity averaged across the sample for the oxygen-partial-pressure range.

As the Sm-doped cerias are mainly ionic conductors under oxidizing conditions, the ambipolar conductivity approximately equals the electronic conductivity ($\sigma_{amb} \approx \sigma_e$), which could be expressed as a combination of p-type and n-type contributions [38]:

$$\sigma_{amb} \approx \sigma_e \approx \sigma_p^0 pO_2^{1/4} + \sigma_n^0 pO_2^{-1/4} \quad (9)$$

where σ_p^0 and σ_n^0 are the p-type and n-type electronic conductivities at $pO_2 = 1$ atm. When permeation is driven by a gradient between oxygen partial pressure pO_2^* at the feed side and pO_2 at the permeate side ($pO_2 < pO_2^*$), Eqs. (2), (7) and (9) yield the following analytical solution:

$$I_p = \frac{A}{L}\frac{RT}{F}\left[\sigma_p^0\left(pO_2^{*1/4} - pO_2^{1/4}\right) + \sigma_n^0\left(pO_2^{-1/4} - pO_2^{*-1/4}\right)\right] \quad (10)$$

Eq. (10) can be rearranged in the following linear representation (Eqs. (11)–(13)) to enable a relatively simple fitting of experimental results:

$$y = \sigma_p^0 x + \sigma_n^0 \quad (11)$$

where x and y corresponds to:

$$y = I_p\frac{LF}{ART\left(pO_2^{-1/4} - pO_2^{*-1/4}\right)} \quad (12)$$

$$x = pO_2^{*1/4}\cdot pO_2^{1/4} \quad (13)$$

This alternative representation in the entire range of the experimental measurements is shown in Fig. 4. The slope and intercept yield the p-type and n-type conductivities at $pO_2 = 1$ atm. The p-type contribution prevails in oxidising conditions, as shown below, and the actual results are quite consistent with results obtained with other methods (Fig. 5).

Though the results in Fig. 4 show the expected trend for $pO_2 \geq 10^{-3}$ atm, this representation also emphasizes important deviations from the assumed simplifications, mainly for relatively low values of pO_2, and at higher T, suggesting prevailing phase transport limitations in diluted conditions, typically for $pO_2 < 10^{-3}$ atm, rather than surface kinetics, which is thermally activated. In fact, gas phase transport limitations are a classical limitation of solid state electrochemical measurements [39,40]. The analysis was, thus, restricted to $pO_2 \geq 10^{-3}$ atm in the reduced side of the cell. The dependence of oxygen flux density of $Ce_{1-x}Sm_xO_{2-\delta}$

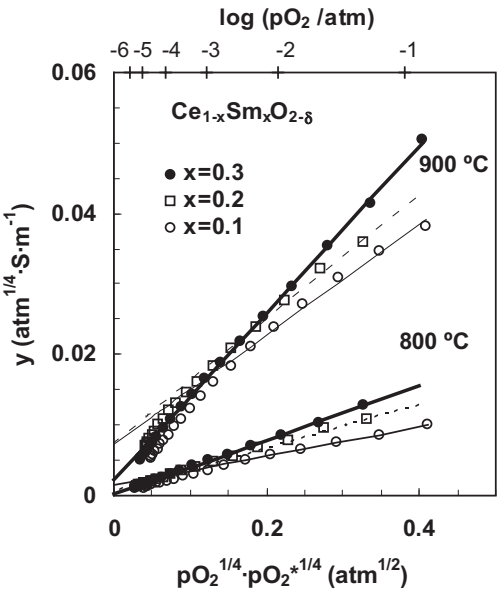

Fig. 4. Alternative representation of the oxygen permeation process according to Eqs. (11)–(13). Points correspond to experimental representation and lines to the lineal fitting in the oxidizing regime.

as a function of the oxygen partial pressure gradient (Fig. 6) also emphasizes the trend towards limiting current values on approaching diluted conditions in the permeate side, suggesting gas phase transport limitations inside the electrochemical cells.

The oxygen-flux density is dependent of the membrane thickness and it is not suitable to compare permeation processes of different samples. A suitable parameter for this purpose is the specific oxygen permeability, defined as [41–43]:

$$J(O_2) = \frac{j_{O_2}\cdot L}{\ln\left(\frac{pO_2^*}{pO_2}\right)} = \frac{RT}{16F^2}\sigma_{amb}^{av} = \frac{RT}{16F^2}t_{o,av}\left(1 - t_{o,av}\right)\sigma_{tot} \quad (14)$$

where $t_{o,av}$ is the ionic transport number averaged across the membrane and σ_{tot} is the overall conductivity. This variable is independent on the membrane thickness when surface limitations are negligible. Otherwise, oxygen surface exchange or other kinetic

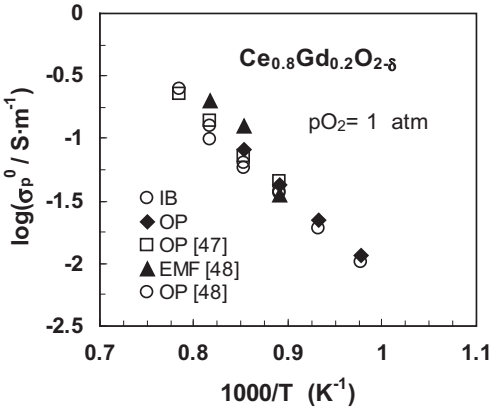

Fig. 5. Arrhenius representation of the p-type electronic conductivity for $Ce_{0.8}Gd_{0.2}O_{2-\delta}$ compared with some bibliographic results. Presented data were obtained by several techniques: IB correspond to an ion-blocking method; OP to an oxygen permeability method and EMF to a modified electromotive force method (Gorelov's modification).

limitations could play a significant role on the overall oxygen flux across the membrane, in addition to the transport properties of the bulk sample [36]. Under these circumstances, Eq. (14) is not satisfied and the specific oxygen permeability should increase with the membrane thickness [42]. Possible ways to enhance the kinetics of the electrochemical reactions at the surfaces are based on porous surface layers and/or an active catalysts [36,37]. Nevertheless, some results previously reported for CGO [27,42] indicated that these materials are not significantly influenced by surface limitations and the oxygen transport should be controlled mainly by the ambipolar conductivity. Regarding this, the authors found that the deposition of porous Pt on the surface of the samples does not play any effect on the overall oxygen flux by permeation. Moreover, similar values of p-type electronic conductivity were obtained for $Ce_{0.8}Gd_{0.2}O_{2-\delta}$ by the use of different and independent electrochemical techniques as modified e.m.f and oxygen permeability [44,45] as is evidenced in Fig. 5. In the mentioned representation we have included the p-type electronic conductivity at $pO_2 = 1$ atm of the same composition prepared by freeze-drying and evaluated by oxygen permeability (current work) and by an ion-blocking method [29]. These evidences confirm a negligible effect of the oxygen surface exchange on the results of permeability. Thus, the main deviations observed for diluted conditions should be mainly due to gas phase transport limitations, possibly depending mainly on the geometry of the cells.

Fig. 7 shows a comparison of the specific oxygen permeability for samples with different contents of Sm, which should be directly related to the ambipolar conductivity averaged across the sample (Eq. (14)). The specific permeability increases when the Sm content increases, mainly for values of pO_2 close to pO_2^*, that is in the regime of moderate oxidizing conditions, suggesting higher values of averaged ambipolar conductivity. On the other hand, Eq. (14) allows one to obtain the ionic transport number averaged across the membrane for a fixed value of oxygen-partial-pressure gradient as represented in Fig. 8 for $Ce_{0.7}Sm_{0.3}O_{2-\delta}$. In this representation, the overall conductivity of the sample was obtained by impedance spectroscopy in air as it is mainly affected by the ionic conductivity in Sm-doped ceria ($\sigma_i >> \sigma_e$), which is assumed as constant in the studied range of oxygen partial pressure. Fig. 8 shows values of $t_0 \geq 0.995$ for temperatures $\leq$900 °C attributable to almost pure ionic conductors under oxidizing conditions. The ionic transport number decreases with increasing oxygen partial pressure in the reduced side of the sample confirming a prevailing p-type component in the electronic transport. Also, this parameter increases by decreasing temperature, suggesting higher activation energy for electronic conduction compared to that of the ionic conduction. Table 1 shows the values of averaged ionic transport number for different samples and temperatures at an approximate oxygen partial pressure gradient $pO_2^*/pO_2 \approx 0.21/0.1$. These results agree very well with those reported by Kharton et al. [46] for

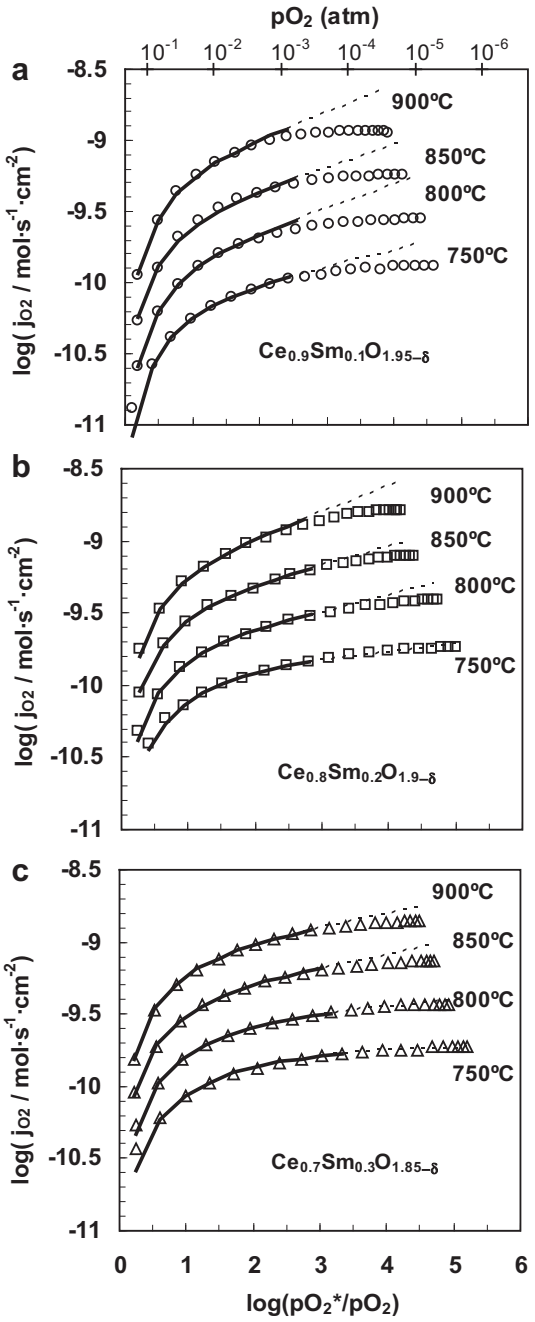

Fig. 6. Oxygen-flux density as a function of the oxygen partial pressure gradient for (a) $Ce_{0.9}Sm_{0.1}O_{1.95-\delta}$, (b) $Ce_{0.8}$ $Sm_{0.2}O_{1.9-\delta}$ and (c) $Ce_{0.7}Sm_{0.3}O_{1.85-\delta}$. Points represent the experimental data and lines the theoretical behaviour according to Eqs. (10)–(13).

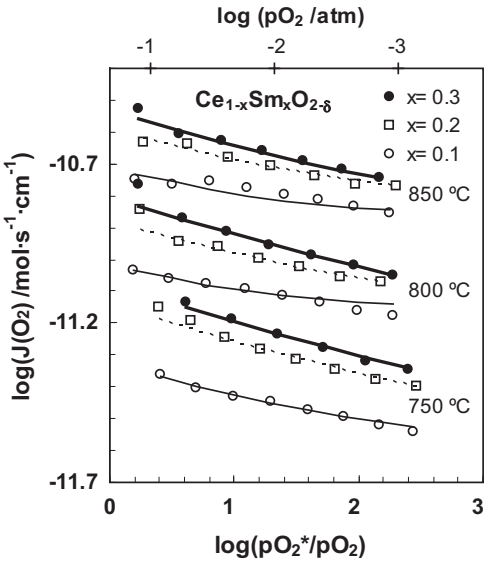

Fig. 7. Specific-oxygen permeability as a function of the oxygen-partial-pressure gradient for different Sm contents and temperatures. Points represent the experimental data and lines the theoretical behaviour.

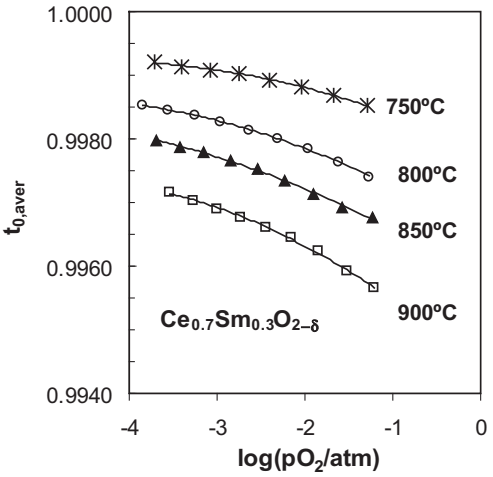

Fig. 8. Ionic transport number of $Ce_{0.7}Sm_{0.3}O_{2-\delta}$ averaged across the sample submitted to a gradient pO_2/0.21 atm as a function of the oxygen partial pressure in the reduced side.

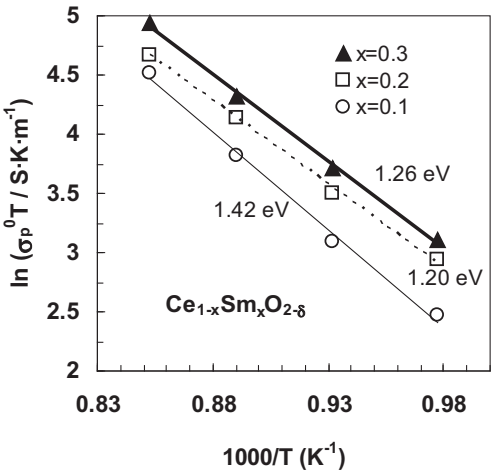

Fig. 9. Arrhenius representation of the p-type electronic conductivity at $pO_2 = 1$ atm.

$Ce_{0.8}Gd_{0.2}O_{2-\delta}$ obtained by a modified e.m.f. (Gorelov's modification) and oxygen permeability.

According to the lineal regression presented in Fig. 4 for the regime of moderate oxidizing conditions, it is apparent that the slope of the fitting increases for higher Sm contents, whereas the intercept follows the opposite trend. Taking into account Eq. (11), the p-type electronic conductivity at $pO_2 = 1$ atm increases with the increase in Sm-contents, while the n-type component decreases. The higher $[Sm'_{Ce}]$ produces higher concentration of positively charged carriers, namely $[V_O^{\bullet\bullet}]$ according to [13]:

$$Sm_2O_3 \rightarrow 2Sm'_{Ce} + V_O^{\bullet\bullet} + 3O_O^X \quad (15)$$

as a consequence the oxygen reaction displaces to the formation of electron holes, thus increasing the p-type conductivity, as follows:

$$\frac{1}{2}O_2(gas) + V_O^{\bullet\bullet} \Leftrightarrow O_O^x + 2h^{\bullet} \quad (16)$$

Table 1
Averaged oxygen-ion transport number for an approximate gradient $pO_2{}^*/pO_2 = 0.21/0.1$ for different compositions and temperatures. Some bibliographic results of $Ce_{0.8}Gd_{0.2}O_{2-\delta}$ obtained from oxygen permeability (OP) and Gorelov's modification of E.M.F.[46] were introduced for comparison.

Sample	T(°C)	$t_{o,av}$
$Ce_{0.9}Sm_{0.1}O_{2-\delta}$	900	0.9941
	850	0.9956
	800	0.9965
	750	0.9968
$Ce_{0.8}Sm_{0.2}O_{2-\delta}$	900	0.9964
	850	0.9973
	800	0.9981
	750	0.9982
$Ce_{0.7}Sm_{0.3}O_{2-\delta}$	900	0.9957
	850	0.9967
	800	0.9974
	750	0.9985
$Ce_{0.8}Gd_{0.2}O_{2-\delta}$	900	0.9968
	850	0.9979
	800	0.9985
	750	0.9990
$Ce_{0.8}Gd_{0.2}O_{2-\delta}$	950	0.993 (OP) [46]
	950	0.991 (EMF) [46]

The dependence of higher p-type electronic conductivity on the contents of Sm is confirmed in the Arrhenius representation at $pO_2 = 1$ atm (Fig. 9). The values of activation energies for the p-type electronic conduction in the range 1.20–1.46 eV extracted from Fig. 9 are in agreement with other values previously reported for several ceria-based materials obtained by different techniques presented in Table 2 [25,38,47–49].

Fig. 10 shows the electronic conductivity of $Ce_{0.7}Sm_{0.3}O_{1.85-\delta}$ as a function of the oxygen-partial pressure under oxidizing conditions obtained from the actual oxygen permeation results, combined with results obtained by ion blocking, for wider ranges of conditions. As an interesting feature, p-type electronic conductivity obtained from the electrochemical permeability in oxidizing conditions, matches very well the ion-blocking results [30], showing the transition from prevailing p-type to prevailing n-type electronic conductivity. This transition is shifted to less reducing conditions with increasing temperature due to the relatively high enthalpy of reducibility relative to creation–annihilation of electrons and holes by band–band transfer [38].

The effect of dopant content on the electrical transport properties of $Ce_{1-x}Sm_xO_{2-\delta}$ is also presented in Fig. 11. The values of ionic conductivity were previously reported for this system [50] and evidenced a great influence of the Sm on the bulk and grain boundary conductivity. Although the sample with lower content of Sm possesses lower p-type electronic conductivity, the very low values of ionic grain boundary conductivity affects its ionic transport number. However, as the ionic conduction is still largely prevailing in air and/or oxygen atmospheres, the p-type electronic conductivity has a negligible effect on the effective open circuit voltage when the materials are used as electrolytes in fuel cells. Moreover, it has been previously stated [15–17] that the

Table 2
Values of activation energy of the electron hole conductivity at $pO_2 = 1$ atm compared with some bibliografic results of several ceria-based compositions.

Sample	Ea (eV)	Technique/Reference
$Ce_{0.8}Sm_{0.2}O_{2-\delta}$	1.20	OP/This work
$Ce_{0.8}Gd_{0.2}O_{2-\delta}$	1.43	OP/This work
$Ce_{0.8}Gd_{0.2}O_{2-\delta}$	1.50	EMF/[45]
$Ce_{0.8}Gd_{0.2}O_{2-\delta}$	1.23	HW/[47]
$Ce_{0.8}Sm_{0.2}O_{2-\delta}$	1.13	HW/[47]
$Ce_{0.8}Sm_{0.2}O_{2-\delta}$	1.24	HW/[48]
$Ce_{0.8}La_{0.2}O_{2-\delta}$	1.26	HW/[47]
$Ce_{0.8}Y_{0.2}O_{2-\delta}$	1.24	HW/[49]

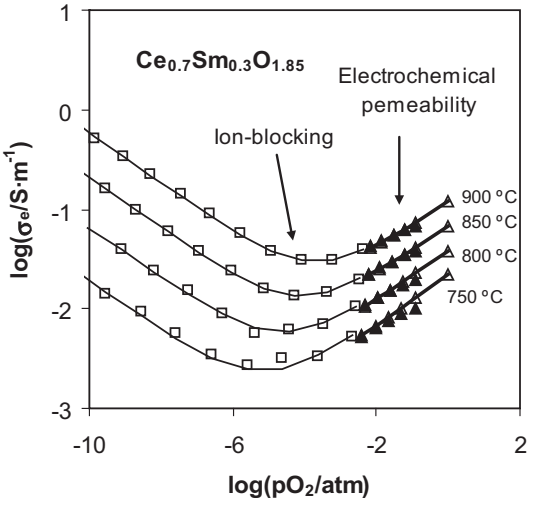

Fig. 10. Total-electronic conductivity as a function of the oxygen partial pressure by oxygen-electrochemical permeability (oxidizing conditions) using Eq. (4) (closed triangles) and using Eq. (9) (open triangles and thick lines). Results of total-electronic conductivity for lower pO_2 from an ion-blocking technique [30] are also represented for comparison (open squares: experimental; thin lines: ±1/4 power law fitting).

enhancement of the electronic conduction around the interface produces an extension of the oxygen exchange surface which improves the electrode kinetics. Regarding this, it was confirmed the enhancement of the electrochemical activity of the interface of Sm-doped ceria electrolytes with a La_2NiO_4 cathode when the Sm content of the electrolyte is higher [51]. For this reason, the optimization of the electrolyte composition in ceria based materials should be based on different properties of the conduction behaviour. The modification of minor electronic transport properties, without important modifications of the overall conductivity under oxidizing conditions, could be a crucial feature in the performance of ceria-based electrochemical cells, or when ceria-based materials are used as buffer layers in contact with the oxygen electrode in SOFC or SOEC systems.

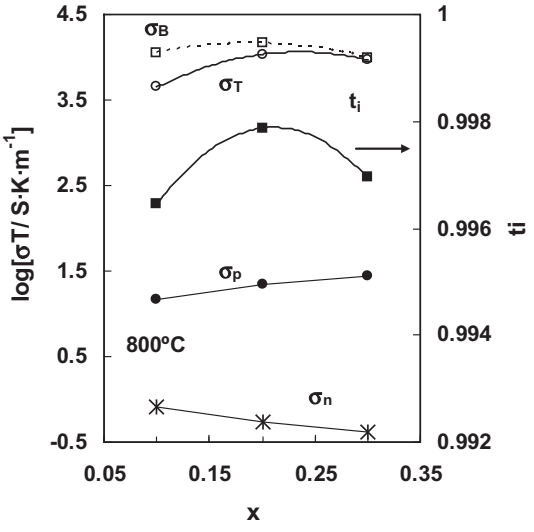

Fig. 11. Ionic (σ_B is bulk conductivity and σ_T is total conductivity) and electronic conductivities (σ_p is p-type electronic conductivity and σ_n is n-type electronic conductivity) at $pO_2 = 0.21$ atm as a function of Sm-content. The ionic transport number estimated from ionic and electronic data at 0.21 atm is represented in the secondary axis.

4. Conclusions

The oxygen-electrochemical permeability has been used to study the mixed conducting behaviour of dense bodies of $Ce_{1-x}Sm_xO_{2-\delta}$ ($x = 0.1, 0.2, 0.3$) under moderate oxidizing conditions (10^{-3}-0.21 atm). The oxygen flux by permeability is highly influenced by the content of Sm in the solid solution. The prevailing ionic conducting character of these materials facilitates the interpretation of ambipolar conductivity, and de-convolution of minor electronic contributions. The p-type character in oxidising conditions yields a slight increase in electronic transport number with increasing oxygen partial pressure. The electronic transport number also increases with temperature due to the lower activation energy of ionic transport compared to that of the electronic transport. Higher additions of samarium enhance the electronic conductivity, in agreement with a higher concentration of p-type carriers predicted by defect chemistry. The p-type electronic transport number remains lower than 0.01 for all compositions in the studied range of T and pO_2. Still, a slight increase in p-type electronic conductivity with negligible effect on the overall ionic transport through the electrolyte may extend the active surface for the electrochemical interchange in the air/oxygen electrodes when ceria-based materials are used as solid electrolytes or buffer layers in high temperature electrochemical cells.

Acknowledgements

Financial assistance of MINECO by means of the project ENE2009-14750-C05-03 is appreciated. D. Pérez-Coll also acknowledges the support provided by the "Ramón y Cajal" Program (MINECO, CSIC). The authors are sincerely grateful to JCC. Abrantes (ESTG-IPVC, Viana do Castelo, Portugal) for the implementation of the "*DC measurement*" software for the automated collection of experimental data.

References

[1] O. Yamamoto, Electrochim. Acta 45 (2000) 2423.
[2] B.C.H. Steele, J. Mater. Sci. 36 (2001) 1053.
[3] A. Hauch, S.D. Ebbesen, S.H. Jensen, M. Mogensen, J. Mater. Chem. 18 (2008) 2331.
[4] S. McIntosh, R.J. Gorte, Chem. Rev. 104 (2004) 4845.
[5] E.V. Tsipis, V.V. Kharton, J. Solid State Electrochem. 12 (2008) 1367.
[6] S.C. Singhal, Solid State Ionics 135 (2000) 305.
[7] N.Q. Minh, Solid State Ionics 174 (2004) 271.
[8] B.C.H. Steele, Solid State Ionics 134 (2000) 3.
[9] Z. Shao, S.M. Haile, Nature 431 (2004) 170.
[10] T. Suzuki, Z. Hasan, Y. Funahashi, T. Yamaguchi, Y. Fujishiro, M. Awano, Science 325 (2009) 852.
[11] H. Inaba, H. Tagawa, Solid State Ionics 83 (1996) 1.
[12] J.W. Fergus, J. Power Sources 162 (2006) 30.
[13] M. Mogensen, N.M. Sammes, G.A. Tompsett, Solid State Ionics 129 (2000) 63.
[14] T. Suzuki, I. Kosacki, H.U. Anderson, J. Am. Ceram. Soc. 85 (6) (2002) 1492.
[15] V.V. Kharton, A.P. Viskup, F.M. Figueiredo, E.N. Naumovich, A.L. Shaula, F.M.B. Marques, Mater. Lett. 53 (2002) 160.
[16] D.P. Fagg, V.V. Kharton, J.R. Frade, J. Solid State Electrochem. 8 (2004) 618.
[17] K. Kakimuna, S. Machida, T. Arisaka, H. Yamamura, T. Akate, Solid State Ionics 176 (2005) 2405.
[18] J.D. Sirman, J.A. Kilner, J. Electrochem. Soc. 143 (1996) L229.
[19] M. Gödickemeier, K. Sasaki, L.J. Gauckler, I. Riess, Solid State Ionics 86-88 (1996) 691.
[20] C. Tian, S.-W. Chan, Solid State Ionics 134 (2000) 89.
[21] T.S. Zhang, J. Ma, L.B. Kong, S.H. Chan, J.A. Kilner, Solid State Ionics 170 (2004) 209.
[22] A. Tschöpe, S. Kilassonia, R. Birringer, Solid State Ionics 173 (2004) 57.
[23] D. Pérez-Coll, P. Núñez, J.C. Ruiz-Morales, J. Peña-Martínez, J.R. Frade, Electrochim. Acta 52 (2007) 2001.
[24] X. Guo, W. Sigle, J. Maier, J. Am. Ceram. Soc. 86 (1) (2003) 77.
[25] S. Lübke, H.-D. Wiemhoefer, Solid State Ionics 117 (1999) 229.
[26] Y. Xiong, K. Yamaji, N. Sakai, H. Kishimoto, T. Horita, M.E. Brito, H. Yokokawa, J. Electrochem. Soc. 153 (12) (2006) A2198.

[27] V.V. Kharton, F.M. Figueiredo, L. Navarro, E.N. Naumovich, A.V. Kovalevsky, A.A. Yaremchenko, A.P. Viskup, A. Carneiro, F.M.B. Marques, J.R. Frade, J. Mater. Sci. 36 (2001) 1105.
[28] D.P. Fagg, I.P. Marozau, A.L. Shaula, V.V. Kharton, J.R. Frade, J. Solid State Chem. 179 (2006) 3347.
[29] D. Pérez-Coll, D. Marrero-López, J.C. Ruiz-Morales, P. Núñez, J.C.C. Abrantes, J.R. Frade, J. Power Sources 173 (2007) 291.
[30] D. Pérez-Coll, A. Aguadero, P. Núñez, J.R. Frade, Int. J. Hydrog. Energy 35 (2010) 11448.
[31] F.M. Figueiredo, V.V. Kharton, A.P. Viskup, J.R. Frade, J. Membr. Sci. 236 (2004) 73.
[32] V.V. Kharton, E.N. Naumovich, A.V. Nikolaev, J. Membr. Sci. 111 (1996) 149.
[33] V.V. Kharton, V.N. Tikhonovich, L. Shuangbao, E.N. Naumovich, A.V. Kovalevsky, A.P. Viskup, I.A. Bashmakov, A.A. Yaremchenko, J. Electrochem. Soc. 145 (4) (1998) 1363.
[34] D. Pérez-Coll, P. Núñez, J.R. Frade, J. Power Sources 196 (2011) 8383.
[35] V.V. Kharton, A.A. Yaremchenko, A.V. Kovalevsky, A.P. Viskup, E.N. Naumovich, P.F. Kerko, J. Membr. Sci. 163 (1999) 307.
[36] J.R. Jurado, F.M. Figueiredo, B. Gharbage, J.R. Frade, Solid State Ionics 118 (1999) 89.
[37] J.R. Jurado, F.M. Figueiredo, J.R. Frade, Solid State Ionics 122 (1999) 197.
[38] M.A. Panhans, R.N. Blumenthal, Solid State Ionics 60 (1993) 279.
[39] F.M.B. Marques, G.P. Wirtz, J. Am. Ceram. Soc. 75 (1992) 369.
[40] F.M.B. Marques, G.P. Wirtz, J. Am. Ceram. Soc. 75 (1992) 375.
[41] V.V. Kharton, A.V. Kovalevsky, A.P. Viskup, A.L. Shaula, F.M. Figueiredo, E.N. Naumovich, F.M.B. Marques, Solid State Ionics 160 (2003) 247.
[42] V.V. Kharton, A.V. Kovalevsky, A.P. Viskup, F.M. Figueiredo, A.A. Yaremchenko, E.N. Naumovich, F.M.B. Marques, J. Electrochem. Soc. 147 (7) (2000) 2814.
[43] D.P. Fagg, S. García-Martín, V.V. Kharton, J.R. Frade, Chem. Mater. 21 (2009) 381.
[44] F.M. Figueiredo, F.M.B. Marques, J.R. Frade, J. Eur. Ceram. Soc. 19 (1999) 807.
[45] V.V. Kharton, A.P. Viskup, F.M. Figueiredo, E.N. Naumovich, A.A. Yaremchenko, F.M.B. Marques, Electrochim. Acta 46 (2001) 2879.
[46] V.V. Kharton, F.M.B. Marques, Solid State Ionics 140 (2001) 381.
[47] Y. Xiong, K. Yamaji, T. Hariza, N. Sakai, J. Electrochem. Soc. 151 (2004) A407.
[48] V. Thangadurai, W. Weppner, Electrochim. Acta 49 (2004) 1573.
[49] Y. Xiong, K. Yamaji, T. Horita, N. Sakai, H. Yokokawa, J. Electrochem. Soc. 149 (2002) E450.
[50] D. Pérez-Coll, P. Núñez, J.R. Frade, J. Electrochem. Soc. 153 (3) (2006) A478.
[51] D. Pérez-Coll, A. Aguadero, M.J. Escudero, P. Núñez, L. Daza, J. Power Sources 178 (2008) 151.